Available online at www.sciencedirect.com
SCIENCE DIRECT®
Geochimica et Cosmochimica Acta 70 (2006) 192–205
Geochimica
www.elsevier.com/locate/gca

Layered mantle structure beneath the western Guyana Shield, Venezuela: Evidence from diamonds and xenocrysts in Guaniamo kimberlites

Daniel J. Schulze [a,*], Dante Canil [b], Dominic M.DeR. Channer [c], Felix V. Kaminsky [d]

[a] Department of Geology, University of Toronto, Erindale College, Mississauga, Ont., Canada L5L 1C6
[b] School of Earth and Ocean Sciences, University of Victoria, Victoria, BC, Canada V8W 3P6
[c] Guaniamo Mining Company, Centro Gerencial Mohedano, La Castellana, Caracas, Venezuela
[d] KM Diamond Exploration, 2446 Shadbolt Lane, West Vancouver, BC, Canada V7S 3J1

Received 25 August 2004; accepted in revised form 2 September 2005

Abstract

Mantle xenoliths and xenocrysts from Guaniamo, Venezuela kimberlites record equilibration conditions corresponding to a limited range of sampling in the lithosphere (100–150 km). Within this small range, however, compositions vary considerably, but regularly, defining a strongly layered mantle sequence. Major and trace element compositions suggest the following lithologic sequence: highly depleted lherzolite from 100 to 115 km, mixed ultra-depleted harzburgite and lherzolite from 115 to 120 km, relatively fertile lherzolite from 120 to 135 km, and mixed depleted harzburgite and relatively fertile lherzolite from 135 to 150 km. Based on comparison with well-documented mantle peridotites and xenocrysts from elsewhere, we conclude that the Meso-proterozoic Cuchivero Province (host to the Guaniamo kimberlites) is underlain by depleted and ultra-depleted shallow Archean mantle that was underplated, and uplifted, by Proterozoic subduction, perhaps more than once. These Proterozoic subduction events introduced less-depleted oceanic lithosphere beneath the Archean section, which remains there and is the source of the abundant Guaniamo eclogite-suite diamonds that have ocean-floor geochemical signatures. Although diamond-indicative low-Ca Cr-pyrope garnets are abundant, they are derived primarily from the shallow depleted layer within the field of graphite stability, and the rare peridotite-suite diamonds are either metastably preserved at these shallow depths, or were derived from the small amount of depleted lithosphere sampled by these kimberlites that remains within the diamond stability field (the mixture of Archean and Proterozoic mantle in the depth range 135–150 km).

1. Introduction

The diamond-rich kimberlite sills, or sheets, of the Guaniamo region of Venezuela contain abundant xenocrysts of low-Ca Cr-pyrope (Nixon et al., 1994; Schulze et al., 2003a). Although elsewhere in the world such a signature is typically associated with an Archean cratonic setting (Griffin et al., 1999a) and an abundance of peridotite-suite diamonds (e.g., Gurney, 1984; Gurney and Zweistra, 1995), this is not the case in Guaniamo. The crystalline basement intruded by the kimberlites belongs to the Proterozoic Cuchivero Province of the Guyana Shield (Sidder and Mendoza, 1995), and almost all of the abundant diamonds (grades are up to 1.5 ct/t—Channer et al., 2001) belong to the eclogite suite (Sobolev et al., 1998; Kaminsky et al., 2000). This is unusual, as kimberlites dominated by eclogitic diamonds, such as those at the Premier and Orapa mines, typically contain relatively few low-Ca Cr-pyropes. Furthermore, with the exception of the Argyle mine in Australia (e.g., Jaques et al., 1989), diamond-rich alkaline volcanic rocks are restricted to Archean cratonic settings. To evaluate the possible causes of the unusual Guaniamo

* Corresponding author. Fax: +1 905 828 3717.
E-mail address: dschulze@utm.utoronto.ca (D.J. Schulze).

0016-7037/$ - see front matter © 2005 Elsevier Inc. All rights reserved.
doi:10.1016/j.gca.2005.08.025

situation, we have investigated the major and trace element compositions of xenocrysts of garnet from the Guaniamo kimberlites. Additional supporting major element data were obtained from a variety of silicate and chromite xenocrysts from these kimberlites. We compare the results from Guaniamo with data from well-studied kimberlites from other tectonic settings.

2. Samples and methods

The major element chemical composition of thousands of xenocrysts of garnet, spinel, and other mantle minerals have been determined by electron microprobe methods as part of the evaluation of the diamond potential of the Guaniamo kimberlite sheets (unpublished data of Guaniamo Mining Company). A small subset of garnets (45 grains) from two of the kimberlites (La Ceniza and Desengano—see Channer et al., 2001), analysed using standard WDS methods with a Cameca SX-50 electron microprobe at the University of Toronto (e.g., Schulze et al., 2003a), have also been analysed for trace elements by LA ICP-MS at the University of Victoria, using methods described in Canil et al. (2003) and references therein. Additional electron microprobe data have been obtained from a single 1 cm garnet peridotite xenolith and various xenocrysts and microxenoliths, including garnet–olivine and chromite-olivine pairs from fresh kimberlite drill core, also using the University of Toronto electron microprobe. The compositions of olivine and chromite inclusions in three Guaniamo diamonds have been obtained by WDS methods using the Cameca SX-100 microprobe at the University of Edinburgh.

The pressures and temperatures of equilibration of these samples have been estimated using a variety of methods. The single clinopyroxene geothermobarometer of Nimis and Taylor (2000) has been applied to Cr-diopside xenocrysts recovered from fresh Guaniamo kimberlite drill core, to determine the thermal regime (paleo-geothermal gradient) in the mantle at the time of kimberlite eruption (approximately 712 Ma ago—see Kaminsky et al., 2004). The partitioning of Ni between garnet and olivine is temperature dependent (Griffin et al., 1989), and we have applied the Ni-in-garnet thermometer of Canil (1999) to our new garnet xenocryst data, and those published for Cr-pyrope inclusions in Guaniamo diamonds. The partitioning of Mg and Fe^{2+} between coexisting olivine and spinel, and between olivine and garnet, is also temperature dependent. We have estimated the equilibration temperatures of Cr-spinel xenocrysts and Cr-spinel diamond inclusions using the formulation of the olivine–spinel Mg–Fe^{2+} thermometer of Poustovetov (2000) and of garnet–olivine pairs using the O'Neill and Wood (1979) method. Estimated depths of origin for samples for which temperature alone was calculated have been obtained by projecting these temperatures onto the paleo-geothermal gradient inferred from Cr-diopside xenocrysts.

3. Results

3.1. Mineral chemistry

The CaO and Cr_2O_3 values of approximately 3000 garnets from eight different kimberlite sills in the Guaniamo region are illustrated in Fig. 1. A very large proportion of these fall into the G10 garnet field. G10 garnets are Cr-pyropes with CaO content so low as to indicate that they are from a harzburgite or dunite paragenesis. They are the most common type of garnet associated with diamonds belonging to the peridotite suite and are of great use in exploring for diamond-bearing kimberlites (Gurney, 1984). Garnets analysed for Si, Ti, Al, Cr, Fe, Mn, Mg, and Ca have been classified using the garnet classification scheme of Schulze (2003). Of the 806 such garnet xenocrysts, 37.9% are classified as derived from harzburgites, 58.8% from lherzolites, 2.6% from eclogites, and 0.7% from wehrlites. No garnets from the Cr-poor megacryst suite were identified.

Compositions of the garnet xenocrysts examined in detail in this study are listed in Table 1 (major elements) and Table 2 (trace elements). Each data set represents a single analysis per grain. Both lherzolite and harzburgite garnets have been analysed from each of the two kimberlite occurrences; La Ceniza ("The Ash") and Desengano ("Disappointment"). There are differences in major element

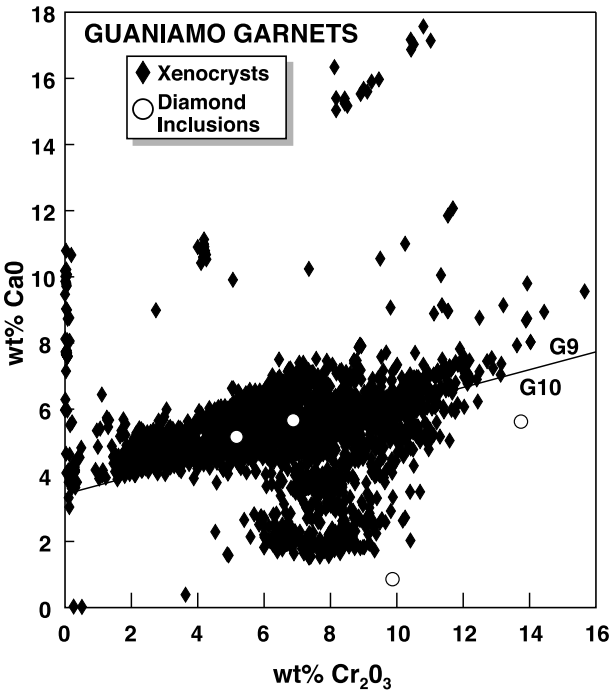

Fig. 1. Plot of CaO vs. Cr_2O_3 for garnet xenocrysts ($n = 2957$) from Guaniamo kimberlites. Data from Schulze et al. (2003a), Kaminsky et al. (2004), this paper, and the unpublished database of the Guaniamo Mining Company. Diamond inclusion data from Nixon et al. (1994) and Kaminsky et al. (2000). Distinction between lherzolite (G9) and harzburgite (G10) garnets taken from Gurney (1984).

Table 1
Major element composition of garnet xenocrysts from La Ceniza and Desengano kimberlites

Sample number	SiO_2	TiO_2	Al_2O_3	Cr_2O_3	FeO[a]	MnO	MgO	CaO	Na_2O	Total	Molar Mg/(Mg + Fe)
La Ceniza lherzolite garnets											
LCG2-A2	41.05	0.04	19.17	6.43	8.14	0.51	17.94	7.09	0.02	100.38	0.797
LCG2-A5	41.54	0.03	20.27	5.37	6.94	0.39	19.23	6.50	0.01	100.28	0.832
LCG2-B1	40.60	0.05	18.71	6.87	8.27	0.60	17.53	7.05	0.01	99.68	0.791
LCG2-B3	40.86	0.07	17.40	8.65	7.58	0.38	18.24	6.68	0.03	99.89	0.811
LCG2-B7	40.94	0.07	17.93	8.51	7.53	0.45	18.71	6.35	0.01	100.50	0.816
LCG2-B8	40.22	0.58	15.01	11.23	7.13	0.39	18.23	6.86	0.10	99.75	0.820
LCG2-B9	41.07	0.11	18.59	7.25	7.38	0.39	19.23	6.08	0.01	100.10	0.823
LCG2-C2	41.91	0.01	21.31	3.98	7.26	0.41	20.04	5.54	0.00	100.46	0.831
LCG2-C4	41.05	0.05	19.44	6.44	7.81	0.44	18.41	6.75	0.01	100.39	0.808
LCG2-C5	41.05	0.07	19.40	6.07	7.81	0.46	18.37	6.66	0.01	99.90	0.807
LCG2-D2	41.08	0.08	19.00	6.50	8.06	0.47	18.07	6.45	0.01	99.70	0.800
LCG2-D5	41.79	0.03	19.38	6.56	7.26	0.39	20.07	5.22	0.03	100.73	0.831
LCG2-D6	41.15	0.05	18.57	7.11	8.30	0.48	17.66	7.43	0.01	100.74	0.791
LCG2-D7	41.14	0.05	19.10	6.68	7.91	0.46	18.08	6.88	0.02	100.32	0.803
La Ceniza harzburgite garnets											
LCG2-A3	41.24	0.12	17.16	9.20	6.82	0.43	21.35	3.36	0.05	99.74	0.848
LCG2-A4	41.14	0.04	18.63	7.37	7.65	0.34	20.27	4.45	0.02	99.92	0.825
LCG2-A6	41.33	0.08	16.74	9.67	7.15	0.36	20.31	4.26	0.05	99.94	0.835
LCG2-B2	41.86	0.08	18.97	7.34	5.92	0.34	22.81	2.22	0.02	99.56	0.873
LCG2-B4	41.89	0.12	20.29	5.57	6.50	0.29	22.22	3.02	0.05	99.94	0.859
LCG2-B5	41.42	0.00	18.70	7.56	7.54	0.37	21.42	2.95	0.01	99.98	0.835
LCG2-B6	40.81	0.18	16.99	9.08	7.26	0.41	19.20	5.74	0.04	99.70	0.825
LCG2-C1	41.93	0.04	19.37	6.74	6.72	0.37	23.20	1.29	0.01	99.67	0.860
LCG2-C3	41.46	0.05	19.01	6.88	7.25	0.38	21.56	3.08	0.04	99.70	0.841
LCG2-C6	41.48	0.04	18.39	7.87	7.65	0.44	21.03	3.64	0.03	100.57	0.831
LCG2-C7	41.80	0.03	18.54	7.65	7.54	0.37	21.03	3.71	0.02	100.68	0.832
LCG2-C8	42.37	0.10	19.95	6.35	6.42	0.29	22.94	2.04	0.05	100.50	0.864
LCG2-C9	43.41	0.04	21.90	4.03	5.68	0.36	24.87	1.21	0.05	101.54	0.886
LCG2-D1	41.19	0.31	18.63	7.06	6.70	0.32	20.51	5.19	0.07	99.97	0.845
LCG2-D3	40.45	0.04	14.33	12.97	7.34	0.38	18.54	6.03	0.03	100.10	0.818
LCG2-D4	41.10	0.10	17.25	9.21	6.89	0.39	21.47	3.33	0.05	99.77	0.847
LCG2-D8	41.75	0.04	18.53	8.09	6.59	0.35	22.84	2.22	0.01	100.41	0.860
LCG2-D9	42.34	0.06	19.14	7.29	6.61	0.27	22.86	2.16	0.02	100.75	0.860
Desengano lherzolite garnets											
DG2-1	41.52	0.35	20.20	4.62	7.36	0.37	19.67	5.05	0.08	99.22	0.826
DG2-3	41.33	0.19	21.32	3.41	8.39	0.38	18.98	5.17	0.06	99.23	0.801
DG2-4	41.89	0.45	22.54	1.61	7.65	0.33	20.53	4.09	0.11	99.20	0.827
DG2-7	41.18	0.08	20.23	4.70	7.76	0.41	18.66	6.08	0.03	99.13	0.811
DG2-9	40.96	0.39	19.55	5.26	8.17	0.40	18.67	5.55	0.07	99.02	0.803
DG2-13	41.29	0.23	22.71	1.50	9.24	0.37	19.09	4.61	0.07	99.12	0.786
DG2-15	41.50	0.22	20.35	4.90	7.86	0.37	19.21	5.47	0.04	99.93	0.813
DG2-16	41.02	0.13	18.46	6.79	7.50	0.39	18.57	6.10	0.04	99.01	0.815
DG2-18	41.62	0.37	21.22	3.38	7.86	0.36	20.17	4.58	0.08	99.64	0.821
Desengano harzburgite garnets											
DG2-2	41.32	0.23	19.78	5.44	7.22	0.39	20.00	4.70	0.06	99.13	0.831
DG2-5	41.65	0.06	18.42	7.70	6.64	0.36	21.59	2.57	0.05	99.04	0.853
DG2-6	42.15	0.00	20.74	4.89	6.76	0.39	22.88	1.61	0.04	99.47	0.858
DG2-11	41.42	0.04	19.48	6.22	7.57	0.34	20.19	4.06	0.05	99.36	0.826
DG2-14	41.36	0.11	19.06	6.55	6.96	0.42	20.03	4.53	0.05	99.04	0.837

Values in weight percent oxides.
[a] Total Fe reported as FeO.

composition between the garnets from the two sills (Table 1), especially in the lherzolite populations. Lherzolitic garnets from La Ceniza tend to have higher Cr contents (mostly >6% Cr_2O_3) whereas most of those from Desengano have <6% Cr_2O_3, suggesting the latter are from less-depleted lithospheric mantle. Although there are few harzburgite garnets analysed from Desengano, that population appears to be compositionally more restricted and does not have the highly magnesian (Mg/(Mg + Fe) > 0.86) and Cr-rich (to 13 wt% Cr_2O_3) garnets present at La Ceniza.

There is a wide variation in trace element compositions within this suite as a whole, but there are also some clear correlations between composition, garnet type, and kimberlite body. In Fig. 2, a comparison of Y vs. Zr, most

Table 2
Trace element composition of garnet xenocrysts from La Ceniza and Desengano kimberlites

Sample	Sc	Ti	V	Ni	Ga	Sr	Y	Zr	Nb	La	Ce	Pr	Nd	Sm	Eu	Gd	Tb	Dy	Ho	Er	Tm	Yb	Lu	Hf	Th	U	Tcanil	Depth
La Ceniza lherzolite garnets																												
LCG2-A2	146	52	146	10	2.0	0.08	1.5	5.2	0.3	0.01	0.09	0.05	0.65	0.23	0.08	0.28	0.04	0.27	0.06	0.18	0.03	0.38	0.08	0.11	55.14	0.01	800	100
LCG2-A5	153	24	100	16	0.8	0.04	2.0	4.9	0.2	0.01	0.09	0.06	0.74	0.43	0.14	0.38	0.05	0.32	0.07	0.28	0.07	0.86	0.21	0.07	2.66	0.01	860	111
LCG2-B1	161	38	148	10	2.0	0.06	0.6	1.7	0.3	0.01	0.09	0.05	0.65	0.27	0.07	0.14	0.02	0.08	0.02	0.09	0.02	0.30	0.07	0.03	2.74	0.01	790	98
LCG2-B3	105	73	181	14	2.6	0.09	0.9	4.4	0.5	0.01	0.15	0.08	0.84	0.34	0.10	0.25	0.03	0.18	0.03	0.10	0.02	0.19	0.04	0.10	1.57	0.01	850	108
LCG2-B7	114	38	185	17	2.4	0.10	0.8	3.5	0.3	0.01	0.33	0.16	1.30	0.32	0.10	0.26	0.03	0.16	0.03	0.08	0.02	0.18	0.04	0.06	1.28	0.01	870	113
LCG2-B8	119	336	219	19	5.1	1.72	7.9	46.9	0.4	0.12	2.15	0.83	7.26	3.24	0.99	2.83	0.33	1.72	0.27	0.67	0.09	0.58	0.08	0.94	0.51	0.05	890	118
LCG2-B9	97	84	214	19	5.0	1.05	3.4	6.0	0.4	0.07	0.78	0.28	2.39	0.60	0.21	0.41	0.06	0.43	0.12	0.47	0.09	0.80	0.14	0.17	0.52	0.01	890	118
LCG2-C2	84	27	122	16	1.9	0.04	1.3	1.0	0.3	0.00	0.07	0.03	0.34	0.11	0.04	0.10	0.01	0.12	0.05	0.22	0.06	0.63	0.12	0.02	3.32	0.01	860	112
LCG2-C4	124	32	152	12	1.7	0.07	0.9	1.0	0.3	0.01	0.13	0.05	0.34	0.07	0.02	0.04	0.01	0.09	0.03	0.18	0.04	0.45	0.09	0.02	2.28	0.01	820	102
LCG2-C5	117	44	157	12	1.9	0.08	0.5	1.9	0.3	0.01	0.10	0.05	0.47	0.10	0.03	0.08	0.01	0.07	0.02	0.09	0.02	0.29	0.07	0.06	1.38	0.01	830	104
LCG2-D2	104	70	150	10	3.0	0.07	2.5	8.5	0.3	0.01	0.08	0.04	0.60	0.60	0.25	0.59	0.07	0.41	0.10	0.36	0.06	0.61	0.11	0.14	1.83	0.01	800	100
LCG2-D5	89	25	156	18	2.8	0.08	1.0	0.8	0.4	0.01	0.22	0.10	0.82	0.08	0.02	0.05	0.01	0.09	0.03	0.15	0.03	0.38	0.07	0.02	1.63	0.01	880	115
LCG2-D6	163	34	173	11	1.9	0.09	0.5	1.7	0.3	0.03	0.21	0.07	0.49	0.11	0.03	0.07	0.01	0.08	0.02	0.09	0.02	0.32	0.08	0.03	0.89	0.01	810	102
LCG2-D7	132	51	138	11	1.9	0.06	1.0	3.2	0.3	0.01	0.08	0.04	0.63	0.32	0.09	0.21	0.03	0.18	0.04	0.13	0.03	0.33	0.07	0.07	0.79	0.01	810	102
La Ceniza harzburgite garnets																												
LCG2-A3	123	79	194	20	2.6	0.86	2.4	18.4	0.4	0.03	0.42	0.18	2.07	1.62	0.55	1.67	0.17	0.72	0.10	0.20	0.03	0.28	0.07	0.30	6.50	0.01	900	119
LCG2-A4	118	29	183	17	1.8	2.77	0.7	3.8	0.3	0.02	0.28	0.13	1.06	0.26	0.07	0.22	0.02	0.13	0.02	0.09	0.02	0.27	0.07	0.10	2.86	0.00	870	113
LCG2-A6	138	67	167	19	3.2	0.23	1.2	8.6	0.5	0.05	0.51	0.21	2.15	0.70	0.18	0.49	0.05	0.26	0.04	0.12	0.02	0.23	0.06	0.20	0.94	0.02	890	117
LCG2-B2	83	59	140	20	1.6	1.48	2.4	30.5	0.3	0.03	0.48	0.23	2.30	1.01	0.32	1.05	0.14	0.70	0.09	0.18	0.02	0.13	0.03	0.61	6.59	0.01	900	119
LCG2-B4	174	225	321	45	9.2	6.07	8.0	83.3	0.7	0.13	1.71	0.58	4.95	2.55	0.92	3.07	0.33	1.58	0.28	0.96	0.17	1.61	0.30	1.38	4.02	0.01	1040	149
LCG2-B5	118	21	179	19	1.8	0.80	0.3	2.9	0.4	0.06	0.72	0.20	1.10	0.16	0.04	0.09	0.01	0.06	0.01	0.05	0.01	0.22	0.05	0.06	1.73	0.01	880	116
LCG2-B6	103	120	189	17	3.7	0.25	3.1	11.4	0.3	0.02	0.30	0.18	2.15	0.91	0.28	0.82	0.11	0.65	0.11	0.29	0.04	0.35	0.07	0.25	0.82	0.01	870	113
LCG2-C1	112	26	152	19	1.6	0.77	0.7	8.2	0.3	0.05	0.89	0.29	1.83	0.39	0.09	0.24	0.03	0.14	0.02	0.08	0.02	0.25	0.07	0.16	2.19	0.01	890	117
LCG2-C3	103	43	173	19	2.7	0.17	1.6	2.7	0.3	0.01	0.15	0.06	0.46	0.17	0.06	0.20	0.03	0.24	0.05	0.21	0.04	0.46	0.09	0.07	2.43	0.00	880	116
LCG2-C6	129	28	184	19	1.7	3.22	0.8	11.8	0.3	0.03	0.47	0.24	2.39	0.55	0.13	0.35	0.04	0.17	0.03	0.08	0.01	0.18	0.05	0.30	0.86	0.00	890	117
LCG2-C7	127	32	177	19	2.0	5.10	1.3	10.3	0.3	0.07	0.93	0.33	2.71	0.68	0.15	0.47	0.06	0.30	0.05	0.12	0.02	0.24	0.06	0.33	1.81	0.00	880	116
LCG2-C8	89	66	156	22	2.0	1.57	1.8	21.3	0.4	0.04	0.64	0.20	1.75	0.92	0.32	0.95	0.11	0.48	0.07	0.18	0.03	0.18	0.04	0.41	0.77	0.01	910	121
LCG2-C9	50	54	119	36	3.9	0.83	0.7	7.9	0.5	0.12	0.67	0.17	1.42	0.42	0.11	0.29	0.03	0.15	0.03	0.06	0.01	0.06	0.01	0.16	0.81	0.01	990	139
LCG2-D1	86	226	193	19	5.1	0.52	7.2	30.9	0.3	0.02	0.34	0.19	2.75	2.32	0.74	2.09	0.23	1.38	0.28	0.84	0.12	0.97	0.15	0.58	1.86	0.01	890	117
LCG2-D3	222	43	172	19	2.0	0.66	1.0	3.2	0.5	0.06	0.65	0.17	1.05	0.23	0.08	0.19	0.03	0.20	0.04	0.12	0.02	0.26	0.05	0.06	0.32	0.01	890	117
LCG2-D4	118	76	177	20	2.7	1.28	2.3	18.0	0.4	0.03	0.47	0.19	2.15	1.67	0.57	1.67	0.17	0.72	0.09	0.20	0.03	0.29	0.06	0.28	1.81	0.01	900	118
LCG2-D8	136	24	177	19	2.4	1.16	0.9	2.8	0.4	0.07	1.01	0.23	1.36	0.25	0.06	0.17	0.02	0.13	0.03	0.13	0.03	0.30	0.07	0.05	2.11	0.01	890	117
LCG2-D9	128	22	167	19	2.4	1.02	0.8	2.6	0.3	0.06	0.90	0.20	1.17	0.21	0.05	0.15	0.02	0.11	0.03	0.12	0.02	0.29	0.07	0.04	0.50	0.01	890	117
Desengano lherzolite garnets																												
DG2-1	111	347	263	36	8.5	0.40	9.1	59.4	0.2	0.02	0.32	0.12	1.22	0.83	0.35	1.21	0.24	1.66	0.32	1.02	0.15	1.17	0.18	1.29	0.00		1000	140
DG2-3	108	207	214	27	7.8	0.07	13.4	13.3	0.2	0.01	0.04	0.02	0.23	0.44	0.28	1.18	0.24	2.08	0.47	1.55	0.27	1.98	0.30	0.24	0.00	0.00	950	129
DG2-4	73	514	236	47	13.1	0.16	12.1	15.2	0.1	0.00	0.10	0.04	0.50	0.49	0.29	1.25	0.24	1.90	0.49	1.43	0.21	1.78	0.26	0.27	0.01	0.01	1040	151
DG2-7	136	118	289	30	4.1	0.20	3.2	11.8	0.3	0.00	0.19	0.10	1.25	0.63	0.27	0.56	0.08	0.49	0.13	0.38	0.08	0.73	0.15	0.40		0.01	960	133
DG2-9	109	363	271	34	10.1	0.21	11.3	21.4	0.2	0.02	0.22	0.11	1.36	1.23	0.50	1.70	0.29	1.86	0.44	1.34	0.19	1.57	0.23	0.56	0.01	0.01	990	138
DG2-15	110	212	257	24	7.1	0.08	9.3	8.1	0.2	0.01	0.06	0.04	0.40	0.33	0.20	0.91	0.20	1.54	0.37	1.09	0.17	1.34	0.21	0.27	0.01	0.01	920	124
DG2-16	154	142	307	30	3.9	0.41	4.0	18.5	0.3	0.01	0.13	0.14	2.42	1.78	0.61	1.87	0.22	1.16	0.16	0.33	0.06	0.49	0.11	0.49	0.01	0.08	960	133
DG2-18	93	382	238	37	10.3	0.08	11.7	16.5	0.2	0.01	0.06	0.02	0.29	0.40	0.23	1.04	0.21	1.90	0.46	1.35	0.21	1.62	0.26	0.34	0.02	0.00	1000	141
Desengano harzburgite garnets																												
DG2-2	120	262	288	42	10.0	0.19	9.9	15.2	0.4	0.01	0.16	0.07	0.92	0.77	0.28	1.03	0.18	1.55	0.38	1.29	0.23	1.67	0.26	0.34	0.01	0.01	1030	146
DG2-5	150	46	275	34	5.7	0.38	3.3	11.7	0.5	0.03	0.71	0.25	1.71	0.58	0.20	0.48	0.06	0.47	0.10	0.47	0.09	0.73	0.15	0.27	0.03	0.04	990	138
DG2-11	151	45	365	39	3.8	2.67	0.9	5.8	0.4	0.06	1.00	0.29	2.19	0.50	0.14	0.35	0.03	0.21	0.03	0.11	0.02	0.41	0.10	0.16	0.03	0.01	1010	143
DG2-14	143	115	309	33	5.4	0.26	2.3	12.0	0.5	0.02	0.27	0.12	1.40	0.62	0.20	0.58	0.07	0.52	0.09	0.19	0.03	0.25	0.06	0.33	0.01	0.01	980	136

Values in ppm.

samples cluster at low values for these elements (<4 ppm Y, <31 ppm Zr), a signature of pyrope garnets from peridotites highly depleted in magmaphile (i.e., incompatible) elements (e.g., Griffin et al., 1999c). Most of the harzburgitic garnets from both bodies and all but one of the lherzolitic garnets from La Ceniza are in this group, which is also marked by depletion in Ti and Ga (Table 2). The majority of Desengano lherzolitic garnets, and one harzburgitic garnet, have significantly higher Y contents (9–13 ppm) at similarly low Zr contents (<22 ppm). Four other garnets with intermediate Y contents (5–9 ppm Y) have Zr values ranging up to approximately 90 ppm (Fig. 2) and are enriched in Ti (Table 2).

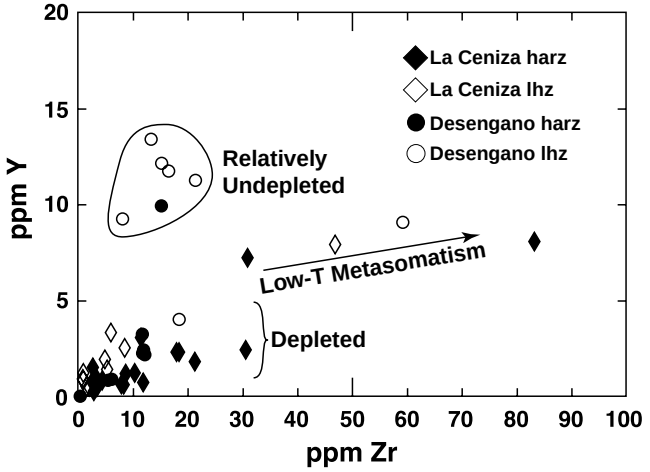

Fig. 2. Compositions of Cr-pyrope xenocrysts from Guaniamo kimberlite in terms of yttrium and zirconium contents. Open symbols represent lherzolitic garnet and filled symbols represent harzburgitic garnets. Diamonds are from La Ceniza and circles are from Desengano. Characterisation as "depleted", "relatively undepleted", and "low-T metasomatism" based on Fig. 13 of Griffin et al. (1999b).

Chondrite-normalised REE patterns of garnets are shown in Fig. 3. Both "normal" patterns for mantle peridotite garnets (LREE-enriched with nearly flat MREE and HREE, and concave downward) and those with "sinusoidal" patterns are present. Most of the La Ceniza garnets, both lherzolitic and harzburgitic, have sinusoidal patterns. The three La Ceniza garnets that are enriched in Zr, with intermediate Y (samples D1, B8, and B4, in the low-T metasomatism group in Fig. 2), have the highest REE values and lack, or have only weakly developed, sinusoidal patterns. The presence of sinusoidal patterns in lherzolite garnets is rare, and thus La Ceniza is unique in this regard. The REE patterns of the Desengano garnets are quite different from that of the La Ceniza suite. Most of the Desengano lherzolitic garnets have normal concave downward patterns, and the "sinuosity" of the others (both lherzolitic and harzburgitic) is not as pronounced as in the garnets from La Ceniza.

The degree of "sinuosity" can be expressed by the $(Nd/Y)_n$ value (Pearson et al., 1998). Garnets with sinusoidal patterns have $(Nd/Y)_n > 1$, and in Fig. 4, comparing $(Nd/Y)_n$ and $(Sc/Y)_n$, all garnets except the Desengano lherzolitic group have $(Nd/Y)_n \geq 1$ and correspond to

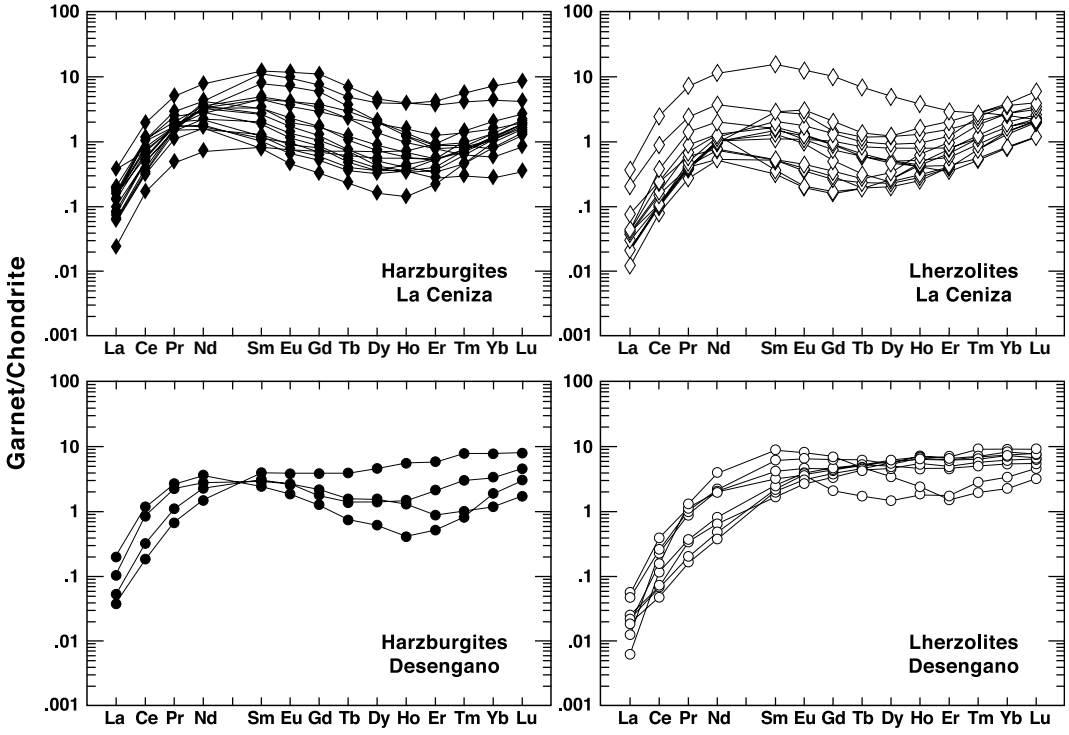

Fig. 3. Chrondrite-normalised rare-earth element patterns for garnets from La Ceniza and Desengano kimberlites, divided into those from lherzolites and those from harzburgites. Note that almost all of the La Ceniza garnets, both from harzburgites and from lherzolites, have "sinusoidal" patterns, as do many from both garnet types at Desengano. Data were normalised using the chondrite values of Sun and McDonough (1989).

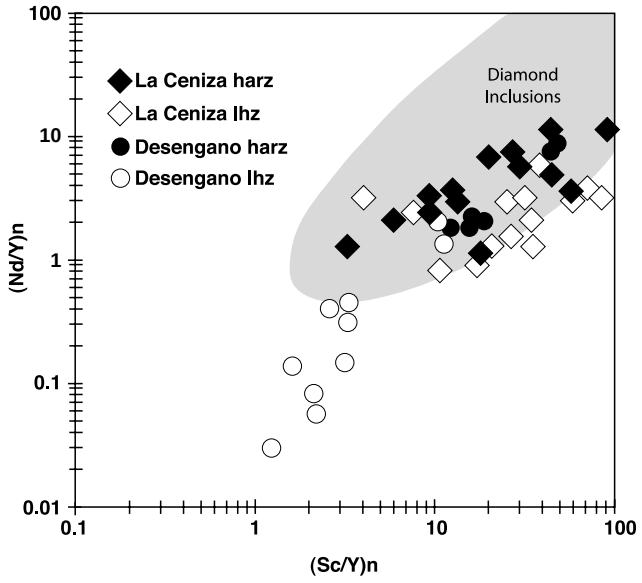

Fig. 4. Chondrite-normalised values of Nd/Y vs. Sc/Y for Guanaimo garnets. The shaded field, "Diamond Inclusions", is from Pearson et al. (1998). Cr-pyropes with $(Nd/Y) \geq 1$, such as those from diamond inclusions, are the most highly depleted in magmaphile elements.

much of the field occupied by Cr-pyrope inclusions in diamonds (Pearson et al., 1998).

Nickel contents are low (10–47 ppm) relative to most mantle garnet populations, indicative of low equilibration temperatures (Griffin et al., 1989; Canil, 1999). In general, La Ceniza Ni values are lower than those from Desengano, the significance of which is discussed below.

Major and minor element compositions of minerals from microxenoliths/composite xenocrysts and the single 1 cm garnet peridotite xenolith are listed in Table 3. The olivine-diopside pair VCX-3 is from the Los Indios ("The Indians") sill, and the other samples are from a concentrate of mixed material from both Los Indios and La Ceniza. Of the five garnet-bearing samples, one is harzburgitic (VX2-A) and the others are lherzolitic. Compositions of the garnets in the xenoliths are within the range of those of the garnet xenocrysts with the exception of those in the garnet lherzolite xenolith, in which all minerals are distinctly more Fe-rich and Cr-poor.

We have also identified three diamonds with peridotite-suite mineral inclusions. The major and minor element compositions of the diamond inclusion olivines and chromites are presented in Tables 4 and 5. Data in Tables 3–5 represent averages of 3–5 points per grain. All minerals appear to be homogeneous. Diamond 13-127-8 has three olivines exposed on its polished surface (Fig. 5A), and on the polished surface of diamond 13-127-17 two olivines in contact with one another are exposed. Within each diamond the olivine compositions are uniform. Those in diamond 13-127-8 have molar $Mg/(Mg + Fe) = 0.947$ and in diamond 13-127-17, molar $Mg/(Mg + Fe) = 0.933$. Prior to polishing diamond 13-127-6, approximately 25 chromites and several olivines were identified within the stone using laser Raman spectroscopy. Five chromites were exposed by polishing of this stone (Fig. 5B). There are minor compositional differences between some of the chromites within this stone,

Table 3
Compositions of minerals from microxenoliths in Guaniamo kimberlites

Sample	Mineral[a]	SiO_2	TiO_2	Al_2O_3	Cr_2O_3	FeO[b]	MnO	MgO	NiO	CaO	Na_2O	ZnO	K_2O	Total	Molar Mg/(Mg + Fe)
VCX-3	ol	41.20	n.a.[c]	n.a.	0.02	7.44	0.09	50.17	0.39	0.02	n.a.	n.a.	n.a.	99.32	0.923
	cpx	54.80	0.31	2.86	1.95	1.96	0.08	15.85	0.07	18.38	2.73	n.a.	0.04	99.03	0.935
VX2-B	ol	41.02	n.a.	n.a.	0.02	7.84	0.09	49.90	0.38	0.02	n.a.	n.a.	n.a.	99.27	0.919
	ga	41.34	0.12	18.71	7.06	7.72	0.42	19.08	0.00	5.62	0.04	n.a.	n.a.	100.12	0.815
VX2-A	ol	41.30	n.a.	n.a.	0.06	6.62	0.07	50.69	0.36	0.01	n.a.	n.a.	n.a.	99.11	0.932
	ga	40.99	0.18	16.41	10.04	6.86	0.42	19.54	0.00	5.48	0.07	n.a.	n.a.	100.00	0.835
VX5-B	ol	41.12	n.a.	n.a.	0.01	7.90	0.08	49.56	0.38	0.02	n.a.	n.a.	n.a.	99.06	0.918
	ga	41.18	0.23	19.31	6.16	7.82	0.42	19.27	0.00	5.46	0.06	n.a.	n.a.	99.91	0.814
VX5-A	ol	40.96	n.a.	n.a.	0.01	7.77	0.09	49.97	0.39	0.02	n.a.	n.a.	n.a.	99.22	0.920
	ga	41.12	0.13	17.56	8.55	7.69	0.42	18.59	0.00	6.36	0.04	n.a.	n.a.	100.44	0.812
VGL-1	ol	40.81	n.a.	n.a.	0.02	8.83	0.08	48.94	0.39	0.02	n.a.	n.a.	n.a.	99.09	0.908
	ga	41.22	0.11	19.81	5.25	9.27	0.51	17.59	0.00	6.28	0.02	n.a.	n.a.	100.06	0.772
	cpx	54.34	0.07	1.53	1.43	1.99	0.08	17.04	0.02	21.75	1.16	n.a.	0.00	99.41	0.939
	cht	0.02	0.66	13.51	49.81	22.42	0.25	10.68	0.09	0.07	n.a.	0.18	n.a.	97.69	
VX6-A	ol	40.81	n.a.	n.a.	0.02	9.80	0.15	48.37	0.37	0.03	n.a.	n.a.	n.a.	99.54	0.898
	cht	0.03	1.11	18.20	46.66	21.01	0.28	11.74	0.13	0.00	n.a.	0.09	n.a.	99.24	
VX6-B	ol	40.91	n.a.	n.a.	0.04	9.85	0.16	48.44	0.37	0.02	n.a.	n.a.	n.a.	99.78	0.898
	cht	0.01	1.12	18.70	45.85	20.96	0.28	12.01	0.13	0.01	n.a.	0.09	n.a.	99.16	
VX6-C	ol	40.83	n.a.	n.a.	0.01	8.69	0.15	49.13	0.38	0.01	n.a.	n.a.	n.a.	99.21	0.910
	cht	0.02	0.54	16.69	49.46	19.54	0.29	11.97	0.09	0.02	n.a.	0.11	n.a.	98.73	
VX6-D	ol	41.20	n.a.	n.a.	0.05	7.82	0.12	49.82	0.39	0.02	n.a.	n.a.	n.a.	99.43	0.919
	cht	0.05	0.27	7.27	61.71	18.21	0.26	11.06	0.08	0.00	n.a.	0.12	n.a.	99.03	

Value in weight percent oxide.
[a] ol, olivine; cpx, clinopyroxene; ga, garnet; cht, chromite.
[b] Total Fe reported as FeO.
[c] n.a., not analysed.

Table 4
Compositions of olivines included within two Guaniamo diamonds

Sample	SiO_2	TiO_2	Cr_2O_3	FeO[a]	MnO	MgO	CaO	NiO	Total	Molar Mg/(Mg + Fe)
13-127-8-1	40.55	0.01	0.02	5.29	0.08	53.09	0.01	0.38	99.04	0.947
13-127-8-2	40.92	0.00	0.02	5.30	0.07	52.95	0.01	0.38	99.28	0.947
13-127-8-3	40.90	0.00	0.02	5.29	0.07	53.24	0.01	0.38	99.54	0.947
13-127-17-1	40.72	0.00	0.03	6.64	0.10	51.75	0.01	0.38	99.25	0.933
13-127-17-2	40.73	0.00	0.04	6.62	0.09	51.79	0.01	0.39	99.27	0.933

Values in weight percent oxide.
[a] Total Fe reported as FeO.

Table 5
Compositions of chromites included in diamond 13-127-6

Grain	SiO_2	TiO_2	Al_2O_3	Cr_2O_3	FeO[a]	MnO	MgO	CaO	ZnO	Total
13-127-6-1	0.06	0.04	5.78	66.46	13.51	0.22	14.70	0.01	0.04	100.82
13-127-6-2	0.07	0.04	6.62	65.06	13.26	0.23	14.93	0.01	0.04	100.24
13-127-6-3	0.06	0.04	6.69	65.50	13.41	0.24	14.83	0.01	0.04	100.82
13-127-6-4	0.07	0.04	6.59	65.07	13.26	0.23	14.86	0.01	0.05	100.17
13-127-6-5	0.07	0.04	6.05	66.32	13.37	0.23	14.70	0.01	0.03	100.82

Values in weight percent oxide.
[a] Total Fe reported as FeO.

especially in Al_2O_3 and Cr_2O_3 contents. Based on cathodoluminescence imaging (Fig. 5B), it appears that grains 2, 3, and 4 are closer to the core than grains 1 and 5, indicating that early formed chromites in this diamond are lower in chromium (molar Cr/(Cr + Al) = 0.868–0.869) than those that formed later (molar Cr/(Cr + Al) = 0.880–0.885). This trend is similar to that described in Yakutian diamonds by Bulanova (1995).

Compositions of chromite xenocrysts from fresh Guaniamo kimberlite drill core (unpublished data of the Guaniamo Mining Company) are illustrated in Fig. 6 in terms of MgO and Cr_2O_3 content, and compared with that of the field of diamond inclusion chromites worldwide and those from Guaniamo diamonds. Though many Guaniamo chromites have Cr_2O_3 values equivalent to those of the diamond inclusion field, they are in general lower in MgO content. Very few (6%) of the Guaniamo chromite xenocrysts plot within the diamond inclusion field, although the chromites included in Guaniamo diamonds all fall within the worldwide diamond inclusion field.

Forty-eight olivine macrocrysts in fresh kimberlite from Los Indios (23 samples) and La Ceniza (25 samples) have been analysed (Fig. 7). Most core compositions cluster in the range Mg/(Mg + Fe) = 0.903–0.934, NiO = 0.34–0.42 wt%, and are interpreted as xenocrysts from disaggregated mantle peridotites. Olivines from 8 of the 10 microxenoliths are within the same range. (Olivines from VX6-A and VX6-B have Mg/(Mg + Fe) = 0.898, NiO—0.37 wt% and may be two fragments of one xenolith.) A compositionally distinct group of rims on the macrocrysts (Mg/(Mg + Fe) = 0.880–0.896, NiO = 0.06–0.37) is interpreted as late overgrowths from the host kimberlite magma undergoing fractionation.

3.2. Equilibration conditions

Five Guaniamo Cr-diopsides (three single cpx grains from Kaminsky et al. (2004), one each from the Cr-diopside/olivine pair and the garnet peridotite in Table 3) meet the criteria of Nimis and Taylor (2000) for using their single crystal Cr-diopside thermobarometer to calculate pressure (P) and temperature (T) conditions of equilibration. Calculated equilibration conditions are in the range 890–1040 °C and 38–45 kbar (Table 6). These points are illustrated in Fig. 8 and are consistent with equilibration on a sub-cratonic geothermal gradient corresponding to a surface heat flow of 40 mW/m^2 (e.g., Pollack and Chapman, 1977). Geothermal gradients estimated using compositions of minerals in garnet peridotite xenoliths from many kimberlites in Archean cratonic settings, worldwide, commonly fit the 40 mW/m^2 heat flow model (e.g., Finnerty and Boyd, 1987). On such a geothermal gradient, the graphite–diamond transition (Kennedy and Kennedy, 1976) occurs at approximately 140 km and 1000 °C (Fig. 8). The uncertainties associated with this thermobarometer (approximately ±5 kbar, ±50 °C—Nimis and Taylor, 2000) allow for a variety of geothermal gradients to be fit to the Cr-cpx data in Fig. 8. The scatter in our P-T points in Fig. 8 approximates that shown by Nimis and Taylor (2000) for Cr-diopsides from kimberlites in Kimberley, South Africa, however, and the geothermal gradient defined for Kimberley by Nimis and Taylor (2000) is quite similar to that determined by Finnerty and Boyd (1987) using conventional pyroxene thermobarometry. Accordingly, we feel that our use of the 40 mW/m^2 trajectory is justified for estimating the depths of origin for other samples for which we have no independent way of determining equilibration pressure (as described below).

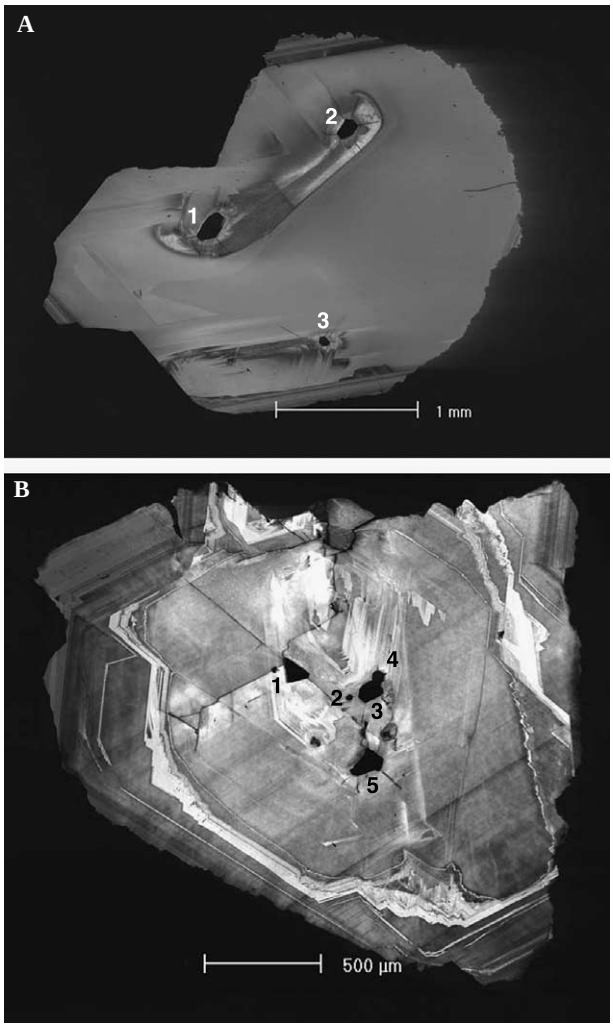

Fig. 5. (A) Cathodoluminescence image of olivine-bearing diamond #13-127-8, cut approximately parallel to (111). The three olivine inclusions (black CL response) have identical compositions (Table 4). The region of the diamond that hosts olivines 1 and 2 appears separated from that hosting olivine 3, although their similar CL patterns suggest that they may be connected in the third dimension and represent an early stage of diamond growth. (B) Cathodoluminescence image of diamond #13-127-6, cut approximately parallel to (111), which contains 5 chromite inclusions near the core. Although the zoning visible in this image does not allow absolute distinction between growth zones in the core, it appears that inclusions 3 and 4 (touching each other) and inclusion 2 occur in a zone closer to the core than do inclusions 1 and 5. There are also compositional distinctions between these two groups, as discussed in the text.

The importance of the Guaniamo Cr-diopside xenocryst compositions corresponding to such a geothermal gradient lies in the fact that these data are the first to constrain a geothermal gradient for the mantle beneath the Guyana Craton in the late Proterozoic. In an earlier study, Nixon et al. (1994) assumed that the abundance of Cr-pyrope xenocrysts with low equilibration temperatures (mostly <1000 °C) necessitated an unusually low geothermal gradient in order to explain the abundance of diamonds in the Guaniamo kimberlites. At that time it was not known that almost all of the Guaniamo diamonds belong to the eclogitic suite and are not related to the Cr-pyrope xenocryst population.

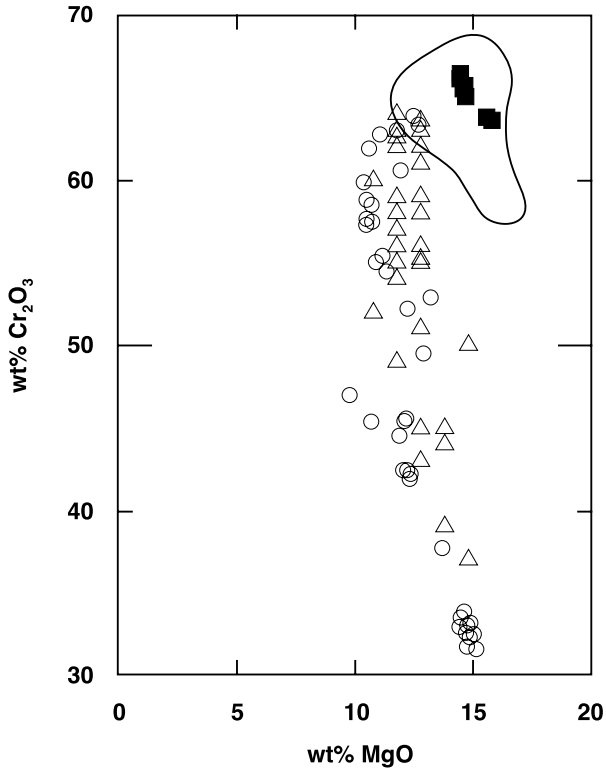

Fig. 6. Compositions of Guaniamo spinels, in terms of MgO and Cr_2O_3 contents. Open symbols represent xenocrysts recovered from fresh kimberlite drill core from La Ceniza (circles) and Los Indios (triangles). Filled symbols represent chromite inclusions in Guaniamo diamonds (Kaminsky et al., 2000; this paper). Solid line represents the field of diamond inclusion chromites worldwide (Geol. Surv. Canada Open File Report 2124, 1989).

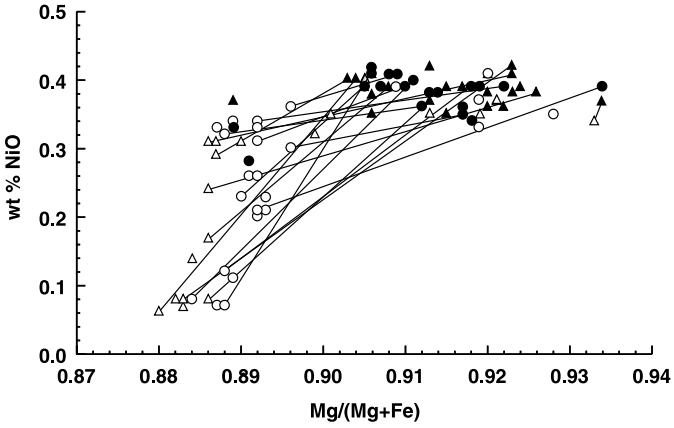

Fig. 7. Compositions of Guaniamo olivine macrocrysts. Solid symbols represent analyses of cores and open symbols represent analyses of rims. Representative core-rim tie-lines are shown. Circles represent olivines from La Ceniza and triangles represent olivines from Los Indios. Note that rims from Los Indios are somewhat more Fe-rich than those from La Ceniza, suggesting that the Los Indios kimberlite was more fractionated than that from La Ceniza at the time of kimberlite eruption.

Temperatures of equilibration for single xenocrysts of Cr-pyrope garnet have been calculated using the Ni-in-garnet thermometer of Canil (1999), which has an uncertainty of approximately ±70 °C (two sigma), equivalent to

Table 6
Equilibration conditions for microxenoliths from Guaniamo kimberlites, using methods described in text

Sample	Temperature NT (2000)[a] (°C)	Pressure NT (2000)[a] (kbar)	Temperature OW (1979)[a] (°C)	Temperature P (2000)[a] (°C)
2[b]	890	41		
3[b]	940	38		
4[b]	1040	42		
VCX-3	940	45		
VX2-B			900	
VX2-A			870	
VX5-B			900	
VX5-A			890	
VGL-1	890	38	820	820
VX6-A				830
VX6-B				840
VX6-C				830
VX6-D				910

[a] NT (2000), Nimis and Taylor (2000); OW (1979), O'Neill and Wood (1979); P (2000), Poustovetov (2000).
[b] Calculated from data in Kaminsky et al. (2004).

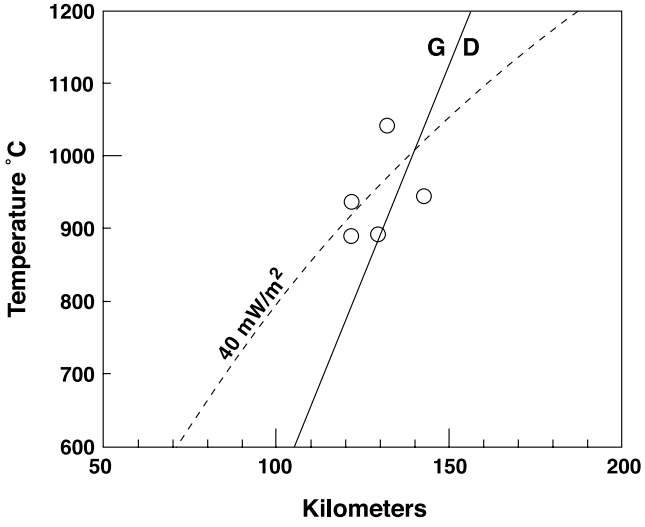

Fig. 8. Equilibration conditions of Cr-diopside xenocrysts from Guaniamo kimberlites, calculated using the method of Nimis and Taylor (2000), using data from Kaminsky et al. (2004) and this paper. For reference, a conductive geotherm corresponding to a surface heat flow of 40 mW/m^2 and the equilibrium boundary between graphite (G) and diamond (D) (Kennedy and Kennedy, 1976) are shown.

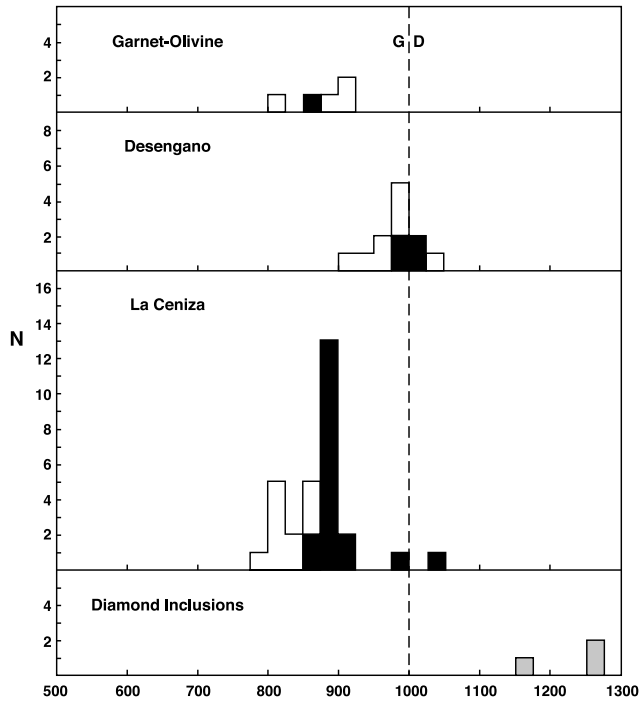

Fig. 9. Temperature distribution of garnet-bearing samples in this study. Temperatures of garnet–olivine pairs derived using the O'Neill and Wood (1979) method, and those from garnet xenocrysts from Desengano and La Ceniza, and from Cr-pyropes included in Guaniamo diamonds, by the Ni-in-garnet method (Canil, 1999). For garnet–olivine pairs and xenocrysts, filled boxes represent harzburgitic garnets and open boxes represent lherzolitic garnets. The graphite (G)–diamond (D) boundary at 1000 °C is taken from Kennedy and Kennedy (1976).

approximately ±15 km in the temperature range applicable to our samples and using the geothermal gradient described above. Although this error introduces uncertainties into the depths quoted below, the relatively small range in major, minor, and trace element compositions of the garnet xenocrysts in our study suggests that there should not be systematic errors related to garnet composition. Thus, the relative depths for various garnet types are likely to be correct. La Ceniza lherzolite garnets yield temperatures in the range 790–890 °C, and those from low-Ca garnet harzburgites are in the range 870–1040 °C (Fig. 9). At Desengano, lherzolite garnets have Ni-in-garnet temperatures in the range 920–1040 °C, and those from harzburgites are in the range 980–1030 °C. Equilibration temperatures calculated for the five garnet–olivine assemblages using the O'Neill and Wood (1979) method, assuming equilibration pressure of 40 kbar, are in the range 820–900 °C. In stark contrast, the Ni-in-garnet temperatures (Canil, 1999) derived from the three published data for Cr-pyrope garnets included within Guaniamo diamonds (Nixon et al., 1994; Kaminsky et al., 2000) are in the significantly higher range of 1170–1260 °C.

Temperatures of equilibration have also been estimated for five chromite-olivine micro-xenolith pairs, for xenocrysts of Cr-spinel, and for Cr-spinel inclusions from Guaniamo diamonds, using the olivine–spinel Mg–Fe^{2+} exchange thermometer, as formulated by Poustovetov (2000). The five olivine-chromite pairs in Table 3 yield equilibration temperatures in the range 820–900 °C (Fig. 10).

For single crystals of Cr-spinel (i.e., chromite xenocrysts and chromite inclusions in diamond), an olivine composition must be assumed to calculate the temperature based on spinel composition alone. Kaminsky et al. (2000) reported that five inclusions of olivine recovered from three Guaniamo diamonds have Mg/(Mg + Fe) values in the range 0.930–0.945. Our new olivine inclusions in Guaniamo diamonds have Mg/(Mg + Fe) values of 0.933 and

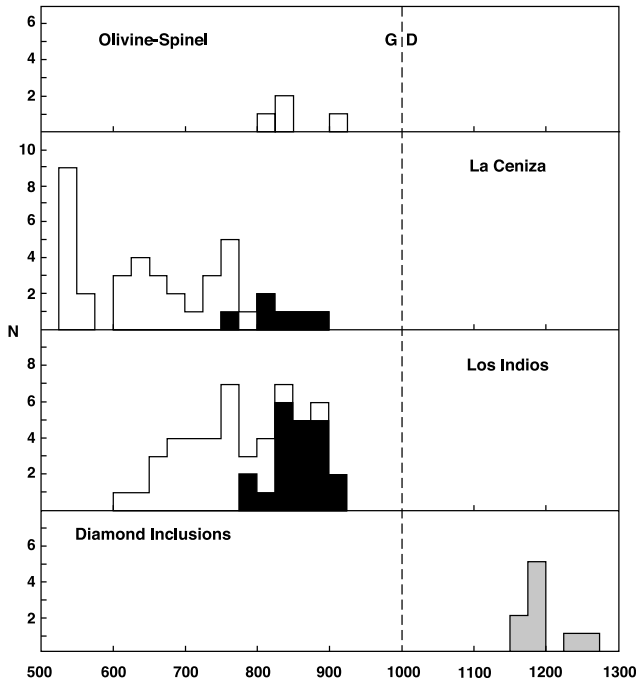

Fig. 10. Temperature distribution of spinel-bearing samples in this study. All temperatures calculated by the method of Poustovetov (2000), as described in the text. For xenocrysts, filled boxes represent grains with >60 wt% Cr_2O_3 and open boxes represent grains with <60 wt% Cr_2O_3. The graphite (G)–diamond (D) boundary at 1000 °C is taken from Kennedy and Kennedy (1976).

0.947 (Table 4). Based on these compositions, we have assumed equilibration of the Cr-spinels with the average composition of Guaniamo diamond inclusion olivine, Fo94, for our equilibration temperature calculations.

With this method, Cr-spinel xenocrysts from fresh Guaniamo kimberlite yield equilibration temperatures in the range <500–910 °C. The more Cr-rich part of the population (wt% Cr_2O_3 in the range 60.0–64.3) is at the hotter end of the spectrum (780–910 °C) than those with Cr_2O_3 values below 60.0 wt% (<500–880 °C) (Fig. 10). The equilibration temperatures of nine Cr-spinels included in Guaniamo diamonds (four published by Kaminsky et al., 2000 and five new analyses from diamond #13-127-6, presented in Table 5) are in the range 1070–1260 °C, substantially higher than the xenocryst temperatures.

With this method, calculated temperatures are very sensitive to choice of olivine composition. Decreasing the forsterite content of the chosen olivine by one mole percent raises the calculated temperature by approximately 50 °C. As the Guaniamo olivine xenocrysts have Mg/(Mg + Fe) in the range 0.903–0.934, the estimated chromite xenocryst temperatures could be too low by as much as 200 °C. Such an error is likely to be more significant for Cr-spinels with lower Cr_2O_3 content (which are likely to have coexisted with less magnesian olivines), and the actual temperature distribution of Cr-spinel xenocrysts is thus probably much like that of the garnet xenocrysts. As the compositional range of olivines included in Guaniamo diamonds is very restricted (Fo 93.0–94.7), the calculated equilibration temperatures for chromite inclusions in diamond (assuming equilibration with olivine of Fo 94.0) are probably within 50 °C of the correct value. Despite the significant errors associated with our application of this thermometer, the Cr-spinel temperature data are essentially in agreement with the results of other thermometry methods. That is, the xenocrysts are cool (below about 900 °C) and the Cr-spinels within the diamonds yield substantially higher equilibration temperatures.

4. Discussion

4.1. Three garnet compositional groupings

The very large proportion of low-Ca Cr-pyropes (G10 garnets) in the Guaniamo kimberlites (Fig. 1) is a characteristic typical of kimberlites that have intruded crust of Archean age and sampled depleted Archean-age lithosphere (e.g., Griffin et al., 1999a). The trace element characteristics of many of the low-Ca Guaniamo garnets, especially those from La Ceniza, indicate extreme depletion in magmaphile elements such as Y, Zr, Ti, and Ga (Table 2, Fig. 2). This depletion exists in lherzolite as well as harzburgite garnets from La Ceniza and, to a lesser extent, Desengano.

Two other distinct groups of garnets are discernible in their trace element compositions. Four garnets with moderate Y and elevated Zr have compositions equivalent to those that Griffin et al. (1999b) concluded have been influenced by the introduction of metasomatising fluids at relatively low temperatures (ca. 1000 °C). In peridotite xenoliths, this type of metasomatic enrichment is commonly accompanied by the introduction of primary metasomatic phlogopite. This style of metasomatism is not restricted to cratonic peridotites of any particular age, and thus cannot be used to distinguish between Archean and Proterozoic mantle samples.

Guaniamo garnets in the third distinct group are characterised by elevated yttrium contents (9–13 ppm Y) at relatively low zirconium values (<22 ppm Zr). These values are intermediate between those in pyropes from Archean-like depleted mantle and garnets from relatively un-depleted mantle from younger regions (e.g., the high-geotherm group in Fig. 13 of Griffin et al., 1999b). This group, represented by Desengano lherzolitic (and one harzburgite) garnets, has trace element characteristics typically associated with peridotitic lithosphere of Proterozoic age (Griffin et al., 1999a), such as Stockdale in North America (Canil et al., 2003).

Although the very extensive database of Griffin et al. (1999a) suggests that the Archean lithospheric mantle is characteristically significantly more depleted than that of Proterozoic age, examples of relatively fertile lithospheric mantle of late-Archean to early-Proterozoic age are known (e.g., Lee et al., 2001). Thus, although the "inferential" dating of the lithospheric mantle using garnet geochemistry seems fairly reliable, it does have limitations. Our interpre-

tation of ages based on garnet chemistry is supported, however, by Sm-Nd model ages previously reported for Guaniamo garnets by Nixon et al. (1994), which is discussed further in Section 4.3 of this paper.

High-temperature (>1200 °C) "melt-metasomatism", caused by interaction of peridotite with asthenosphere-derived magmas, resulting in enriched Ti, Zr, Y, etc., signatures (e.g., Griffin et al., 1999b), is not recognised in the Guaniamo garnet population. This is consistent with the fact that Cr-poor megacryst garnets, another product of these high-temperature magmas, are absent from the Guaniamo kimberlites.

4.2. Mantle structure

The pressures and temperatures of equilibration of the Cr-diopsides, determined by the method of Nimis and Taylor (2000), are consistent with a steady-state conductive geothermal gradient (corresponding to a surface heat flow of approximately 40 mW/m^2) beneath the western Guyana Shield at the time of kimberlite eruption, approximately 712 Ma ago. Projection of equilibration temperatures (derived using methods that do not independently provide a pressure estimate, such as Ni-in-garnet thermometry) onto this geothermal gradient allows estimation of relative depths for origin of the various garnet types. The absence of Cr-poor megacryst garnets and garnets showing evidence of high-temperature melt metasomatism indicates that there is not likely to be a "kinked" or "perturbed" geotherm, the presence of which would add considerable uncertainties to the pressure/depth estimates by this projection.

In Fig. 11, contents of Y (a measure of fertility) and Cr_2O_3 (a measure of depletion level) are shown as they vary with inferred depth of equilibration of the Cr-pyrope xenocrysts. Sampling of mantle material by these two kimberlites extended over approximately 50 km. The La Ceniza kimberlite contains material from the complete range (approximately 100–150 km), though mostly it sampled the shallow portion (<120 km), whereas most of the deep material (120–150 km) is represented by material from the Desengano sill.

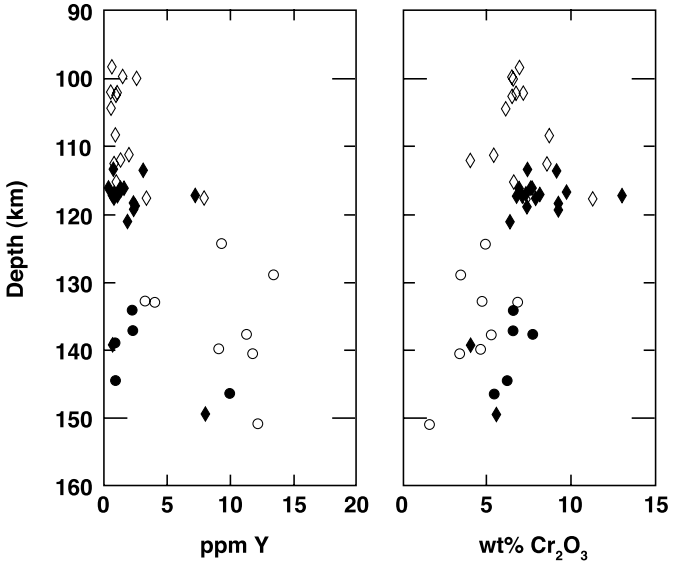

Fig. 11. Variations in yttrium and chromium with inferred depths of origin for Cr-pyrope xenocrysts from La Ceniza (diamonds) and Desengano (circles). Open symbols represent lherzolitic garnets and filled symbols represent harzburgitic garnets.

The mantle sampled by these kimberlites was clearly layered, essentially comprising two repeated sections of lherzolite underlain by mixed lherzolite and harzburgite. The shallowest portion (approximately 100–115 km) contains only highly depleted lherzolites with low Y and moderate Cr contents. Below this, to approximately 120 km, is a mixture of lherzolites and harzburgites, some of which are even more depleted than the shallower lherzolite layer, as they range to higher chromium contents (to 13 wt% Cr_2O_3) at similarly low yttrium levels (<4 ppm Y). This extremely depleted layer is underlain by a mixture of relatively fertile lherzolites (9–13 ppm Y and moderate Cr contents) and depleted harzburgites (<5 ppm Y), with lherzolites dominating the upper portion (120–135 km) of this lower mixed section.

Although we do not have trace element data for the micro-xenoliths in Table 3, there is nothing in their mineral assemblages or major element mineral chemistry that is inconsistent with the trace element—chromium—depth relations described above for the garnet xenocrysts. No xenoliths or xenocrysts with depths of origin greater than 150 km occur in the xenolith/xenocryst suite and thus it appears that the kimberlites began sampling mantle material at that depth.

4.3. Origin of layered mantle beneath Guaniamo

The peridotites represented by garnets from the shallowest portion of the Guaniamo mantle section (<120 km) are among the most strongly depleted garnet peridotites recognised to date (compare with Griffin et al., 1999a). In this regard, they are similar to shallow mantle beneath the central Slave Craton (Griffin et al., 1999c). The Slave Craton is Archean in age, however, and is expected to have depleted mantle beneath it (Griffin et al., 1999a), whereas the western portion of the Guyana Shield, which hosts the Guaniamo kimberlites, contains only Proterozoic rocks at the surface (e.g., Channer et al., 2001). Although Archean rocks are exposed elsewhere on the Guyana Shield (e.g., the Imataca Complex—Montgomery and Hurley, 1978), the Guaniamo kimberlites are located within the Cuchivero Province of the shield (located immediately to the west of the Imataca), which consists of calc-alkaline felsic volcanic rocks and granitic intrusions. Initial strontium isotope ratios ($^{87}Sr/^{86}Sr_i$) of 0.705–0.707 lie between values for Proterozoic crust (>0.708) and mantle magmas (<0.7045), suggesting mostly juvenile continental crust, with some crustal addition (Sidder and Mendoza, 1995), including Archean crust (Santos et al., 2000). Moser (1996) obtained

a U-Pb age of 1864 ± 4 Ma for 10 titanite fragments from crustal inclusions in Guaniamo kimberlite. This age is the only precise U-Pb age for Cuchivero group rocks in Venezuela, as all others are by the alteration-susceptible Rb-Sr method. Based on the worldwide very strong association of highly depleted Ca-poor Cr-pyrope xenocrysts with kimberlites that have sampled Archean lithosphere (Griffin et al., 1999a), the presence of a similarly highly depleted harzburgitic garnet population in the Guaniamo kimberlites implies that there is Archean lithosphere beneath the Proterozoic Cuchivero Province. This is consistent with Sm-Nd model ages of 2.48–2.6 Ga for the highly depleted harzburgitic Cr-pyropes from Guaniamo (Nixon et al., 1994).

The less-depleted to moderately fertile mantle at depths beneath the shallow ultra-depleted Archean layer bears stronger resemblance to the type of lithospheric mantle recognised from studies of numerous kimberlites emplaced through Proterozoic lithosphere (Griffin et al., 1999a; Canil et al., 2003). Although some occurrences of this type of garnet, representing moderately fertile peridotite, are known from kimberlites in an Archean cratonic setting (e.g., Griffin et al., 1994), they are uncommon, and thus we interpret the relatively Y-rich Desengano garnets as representing Proterozoic lithosphere that was present underneath the ultra-depleted Archean lithosphere 700 Ma ago. Most of the Desengano harzburgite garnets are similar to the shallower depleted La Ceniza garnets (<5 ppm Y), and the lowest mantle package in the section sampled by the Guaniamo kimberlites (135–150 km) appears to be a mixture of relatively fertile Proterozoic peridotite and depleted Archean peridotite. This is consistent with Proterozoic Sm-Nd model ages of 1.95–2.36 Ga for lherzolitic Cr-pyropes from Guaniamo (Nixon et al., 1994).

The presence and chemical characteristics of the peridotite diamond inclusion suite in the Guaniamo kimberlites may assist in interpreting geologic evolution of the unusual Guaniamo mantle section. The trace element characteristics of the Cr-pyrope inclusions (e.g.,<5 ppm Y, <20 ppm Zr—Nixon et al., 1994; Kaminsky et al., 2000) are quite similar to those of the ultra-depleted garnet xenocrysts and thus the peridotitic diamonds and ultra-depleted garnet peridotites may be co-genetic. Assuming equilibration on, or near, a steady-state conductive geothermal gradient (c.f. Nimis, 2002), the equilibration temperatures of the diamond inclusion Cr-pyropes and chromites (1070–1260 °C and 1170–1260 °C, respectively) suggest formation at depths of the order of 155–205 km, well within the field of diamond stability (>1000 °C, >140 km).

If the peridotitic diamonds and depleted low-Ca garnet harzburgites have a common origin, substantial cooling has taken place since encapsulation of the peridotite-suite minerals by the diamonds. It is unlikely that the equilibration temperatures of the diamond inclusion garnets and chromites reflect the ambient conditions at the time of kimberlite eruption, as there is no indication in *any* of the other xenocrysts or xenoliths of equilibration at temperatures >1050 °C or depths >150 km. Because of the positive slope of the graphite-diamond transition, simple isobaric cooling following diamond formation would move the rocks further into the field of diamond stability. Cooling during tectonic uplift, however, could move the diamonds and their depleted peridotite hosts to shallower depths indicated by the Ni-in-garnet temperatures, into the graphite stability field, converting the diamonds to graphite, yet allowing the depleted garnet geochemical signature to survive.

A model incorporating our new geochemical data for the mantle beneath the Guaniamo area with the geologic history of the western Guyana Shield is as follows. Diamonds formed in their stability field during the Archean within extremely depleted chromite-bearing low-Ca Cr-pyrope harzburgite. The ultimate origin of this depleted material is unknown, although Griffin et al. (2003) suggested that such depleted rocks formed in the Archean through two regimes, one involving major mantle overturns and another more similar to modern plate tectonics where residues of shallow melting events in an island arc setting were subsequently subducted to depths of diamond stability. The host cratonic block was the Imataca Complex, which was strongly affected by the Trans-Amazonian orogeny (Montgomery and Hurley, 1978) and uplifted to form a mountainous area, the source of many of the detrital zircons in the lower Roraima Formation (ca. 1.9 Ga; Santos et al., 2003). From 2.1 to 1.87 Ga a series of island arcs, the Tapajos-Parima Province (Santos et al., 2000, 2002, 2004) formed to the west of the Archean craton fragments, and arc collision with the Imataca Complex ca. 1.9 Ga may have thrust oceanic lithosphere beneath the Imataca. Santos et al. (2000) suggested that post-collisional Cuchivero Province magmatism was the end result of shallow subduction during accretion of Tapajos-Parima arcs. This magmatism probably thoroughly reworked the collisional zone between Tapajos-Parima arcs and the Imataca complex, as the original lithologies are not preserved at the surface in the Guaniamo region. Present upper crustal structure is constrained by recent seismic studies (Schmitz et al., 2002), which show crustal thickness increasing steadily from 42 km for the Imataca complex to 46 km for the Cuchivero Province, with a sharply defined Moho. Shallow Tapajos-Parima subduction (Santos et al., 2000, 2004) could have underthrust a wide section of Archean mantle, causing ramping of the Archean fragment over the downgoing Proterozoic oceanic lithospheric slab. This further uplift of the Imataca brought the diamond-bearing Archean mantle lithosphere to levels of graphite stability, converting the peridotitic diamonds to graphite. Proterozoic oceanic lithosphere emplaced, and remaining, beneath the uplifted Archean package, and inter-fingered with remnants of depleted Archean lithosphere below 135 km, is the source of the abundant eclogite-suite Guaniamo diamonds that have carbon and oxygen isotope compositions indicative of formation from subducted oceanic material (Sobolev et al., 1998; Kaminsky et al., 2000; Schulze et al., 2003a,b). A Proterozoic Ar–Ar age for an eclogitic clinopyroxene inclusion in a Guaniamo diamond (P.H.

Nixon and R. Burgess, personal communication) is consistent with the Proterozoic subduction event recognised from surficial geology (Santos et al., 2004). The measured Bouguer gravity anomaly along an east–west seismic line from the Imataca complex across the Cuchivero province is quite different from the calculated anomaly, and Schmitz et al. (2002) attributed the difference to higher density material, such as subducted oceanic crust, in the mantle beneath the Cuchivero province (consistent with the above arguments). The few peridotite-suite diamonds that occur in the Guaniamo kimberlites either represent metastable survivors within the shallow depleted low-Ca Cr-pyrope peridotite near 120 km, or were derived from within their stability field in the depleted Archean mixed with the Proterozoic material at about 140–150 km.

Collisional tectonics continued on the western edge of the Guyana Shield in the Meso- and Neo-Proterozoic, with the Rio Negro province forming and accreting between 1.85 and 1.56 Ga. Major intra-plate mafic tholeiitic magmatism occurred across the Amazon Craton from 1.785–1.780 Ga (Avanavero suite; Santos et al., 2002) and was associated with continental rifting. Post-collisional granitic magmatism continued in Guaniamo until around 1.4 Ga (Moser, 1996). Finally, the Sunsas event (Grenvillian) from 1.33 to 0.99 Ga, caused by collision even further west, caused north-east directed faulting and shearing throughout the craton, and reset Ar–Ar and Rb–Sr isotopic systems. Alkaline mafic and syenitic rocks were emplaced in Guaniamo during this event, part of the Cachoeira Seca suite (Santos et al., 2002). These later orogenic events were located too far to the west and are too young to have played a role in the development of the mantle structure beneath Guaniamo. However, all of these events left their mark in the Guaniamo region which, as with other diamondiferous kimberlite provinces, is characterised by high magmatic and structural permeability (Kaminsky et al., 1995; Vearncombe and Vearncombe, 2002).

Acknowledgements

We are very grateful to Mr. Robert E. Cooper, President of the Guaniamo Mining Company, for his determination and support, which have made this work possible. We also thank Claudio Cermignani, Adrian van Rythoven, Nicola Cayzer, R. Cox, and Alison Dias for technical assistance. Reviews by Cin-Ty Lee and Thomas Stachel helped to improve the manuscript. DJS and DC thank NSERC for financial support.

Associate editor: Clive R. Neal

References

Bulanova, G.P., 1995. The formation of diamond. *J. Geochem. Explor.* **53**, 1–24.

Canil, D., 1999. The Ni-in-garnet geothermometer: calibration at natural abundances. *Contrib. Mineral. Petrol.* **136**, 240–246.

Canil, D., Schulze, D.J., Hall, D., Hearn, B.C., Milliken, S.M., 2003. Lithospheric roots beneath western Laurentia: the geochemical signal in mantle garnets. *Can. J. Earth Sci.* **40**, 1027–1051.

Channer, D.M.DeR., Egorov, E., Kaminsky, F., 2001. Geology and structure of the Guaniamo diamondiferous kimberlite sheets, southwest Venezuela. *Revista Brasiliera de Geociencias* **31**, 615–630.

Finnerty, A.A., Boyd, F.R., 1987. Thermobarometry for garnet peridotites: basis for the determination of thermal and compositional structure of the upper mantle. In: Nixon, P.H. (Ed.), *Mantle Xenoliths*. Wiley, London, pp. 381–402.

Geologic Survey of Canada. 1989. The development of advanced technology to distinguish between diamondiferous and barren diatremes. Open File Report 2124.

Griffin, W.L., Ryan, C.G., Cousens, D.C., Sie, S.H., Suter, G.F., 1989. Ni in Cr-pyrope garnets: a new geothermometer. *Contrib. Mineral. Petrol.* **103**, 199–202.

Griffin, W.L., Sobolev, N.V., Ryan, C.G., Pokhilenko, N.P., Win, T.T., Yefimova, E.S., 1994. Trace elements in garnets and chromites: diamond formation in the Siberian lithosphere. *Lithos* **29**, 235–256.

Griffin, W.L., Fisher, N.I., Friedman, J., Ryan, C.G., O'Reilly, S.Y., 1999a. Cr-pyrope garnets in the lithospheric mantle: compositional systematics and relation to tectonic setting. *J. Petrol.* **40**, 679–704.

Griffin, W.L., Shee, S.R., Ryan, C.G., Win, T.T., Wyatt, B.A., 1999b. Harzburgite to lherzolite and back: metasomatic processes in xenoliths from the Wesselton kimberlite, Kimberley, South Africa. *Contrib. Mineral. Petrol.* **134**, 232–250.

Griffin, W.L., Doyle, B.J., Ryan, C.G., Pearson, N.J., O'Reilly, S.Y., Kivi, K., van Achterbergh, E., Natapov, L.M., 1999c. Layered mantle lithosphere in the Lac de Gras area, Slave Craton: composition, structure and origin. *J. Petrol.* **40**, 704–727.

Griffin, W.L., O'Reilly, S.Y., Abe, N., Aulbach, S., Davies, R.M., Pearson, N.J., Doyle, B.J., Kivi, K., 2003. The origin and evolution of Archean lithospheric mantle. *Precamb. Res.* **127**, 19–41.

Gurney, J.J. 1984. A correlation between garnets and diamonds. In: Glover, J.E., Harris, P.G. (Eds.), *Kimberlite Occurrence and Origin: A Basis for Conceptual Models in Exploration*. University of Western Australia Publication 8, pp. 376–383.

Gurney, J.J., Zweistra, P., 1995. The interpretation of the major element compositions of mantle minerals in diamond exploration. *J. Geochem. Expl.* **53**, 293–309.

Jaques, A.L., Hall, A.E., Sheraton, J.W., Smith, C.B., Sun, S-S., Drew, R.M., Foudoulis, C., Ellingsen, K., 1989. Composition of crystalline inclusions and C-isotopic composition of Argyle and Ellendale diamonds. In: Ross, J. (Ed.), *Kimberlites and Related Rocks. Their Mantle/Crust Setting, Diamonds and Diamond Exploration*, vol. 2. Blackwell, Carlton, Australia, pp. 966–989.

Kaminsky, F.V., Feldman, A.A., Varlamov, V.A., Boyko, A.N., Olofinsky, L.N., Shofman, I.L., Vaganov, V.I., 1995. Prognostication of primary diamond deposits. *J. Geochem. Expl.* **53**, 167–182.

Kaminsky, F.V., Zakharchenko, O.D., Griffin, W.L., Channer, D.M.DeR., Khachatrayan-Blinova, G.K., 2000. Diamond from the Guaniamo area, Venezuela. *Can. Mineral.* **38**, 1347–1370.

Kaminsky, F.V., Sablukov, S.M., Sablukova, L.I., Channer, D.M.DeR., 2004. Neoproterozoic "anomalous" kimberlites of Guaniamo, Venezuela: mica kimberlites of "isotopic transitional" type. *Lithos.* **76**, 565–590.

Kennedy, C.S., Kennedy, G.C., 1976. The equilibrium boundary between graphite and diamond. *J. Geophys. Res.* **81**, 2467–2470.

Lee, C.-T., Yin, Q., Rudnick, R.L., Jacobsen, S.B., 2001. Preservation of ancient and fertile lithospheric mantle beneath the southwestern United States. *Nature* **411**, 69–73.

Montgomery, C.W., Hurley, P.M., 1978. Total rock U-Pb and Rb-Sr systematics in Imataca Series, Guyana Shield, Venezuela. *Earth Planet. Sci. Lett.* **39**, 281–290.

Moser, D.E., 1996. *Report on Rb-Sr and U-Pb Geochronology of Kimberlite Sample GL-1 and Granite Sample Guan-1*. Report for Guaniamo Mining Company, Caracas, Venezuela.

Nimis, P., 2002. The pressures and temperatures of formation of diamond based on thermobarometry of chromian diopside inclusions. *Can. Mineral.* **40**, 871–884.

Nimis, P., Taylor, W.R., 2000. Single clinopyroxene thermobarometry for garnet peridotites. Part 1. Calibration and testing of a Cr-in-cpx barometer and an enstatite-in-cpx thermometer. *Contrib. Mineral. Petrol.* **139**, 541–554.

Nixon, P.H., Griffin, B.L., Davies, G., Condliffe, E., 1994. Cr-garnet indicators in Venezuela kimberlites and their bearing on the evolution of the Guyana Craton. In: Meyer, H.O.A., Leonardos, O.H. (Eds.), *Kimberlites, Related Rocks and Mantle Xenoliths*. C.P.R.M. Spec. Pub. 1/A, Brasilia, pp. 378–387.

O'Neill, H.St.C., Wood, B.J., 1979. An experimental study of Fe-Mg partitioning between garnet and olivine and its calibration as a geothermometer. *Contrib. Mineral. Petrol.* **70**, 59–70.

Pearson, N.J., Griffin, W.L., Kaminsky, F.V., van Achterbergh, E., O'Reilly, S.Y., 1998. Trace element discrimination of garnet from diamondiferous kimberlites and lamproites. Ext. Abstr. 8IKC, Cape Town, 673–675.

Pollack, H.N., Chapman, D.S., 1977. On the regional variation of heat flow, geotherms and lithospheric thickness. *Tectonophysics* **38**, 279–296.

Poustovetov, A., 2000. Numerical modelling of chemical equilibria between chromian spinel, olivine and basaltic melt with petrological applications. Ph.D. Thesis, Queens University, Kingston.

Santos, J.O.A., Hartmann, L.A., Gaudette, H.E., Groves, D.I., McNaughton, N.J., Fletcher, I.R., 2000. A new understanding of the provinces of the Amazon Craton based on integration of field mapping and U-Pb and Sm-Nd geochronology. *Gondwana Res.* **3**, 453–488.

Santos, J.O.A., Hartmann, L.A., McNaughton, N.J., Fletcher, I.R., 2002. Timing of mafic magmatism in the Tapajos province (Brazil) and implications for the evolution of the Amazon Craton: evidence from baddelyite and zircon U-Pb SHRIMP geochronology. *J. South Am. Earth Sci.* **15**, 409–429.

Santos, J.O.A., Potter, P.E., Reis, N.J., Hartmann, L.A., Fletcher, I.R., McNaughton, N.J., 2003. Age, source, and regional stratigraphy of the Roraima Supergroup and Roraima-like outliers in northern South America based on U-Pb geochronology. *Geol. Soc. Am. Bull.* **115**, 331–348.

Santos, J.O.A., van Breeman, O.B., Groves, D.I., Hartmann, L.A., Almeida, M.E., McNaughton, N.J., Fletcher, I.R., 2004. Timing and evolution of multiple Paleoproterozoic magmatic arcs in the Tapajos domain, Amazon Craton: Constraints from SHRIMP and TIMS zircon, baddelyite, and titanite U-Pb geochronology. *Precambrian Res.* **131**, 73–109.

Schmitz, M., Chalbaud, D., Castillo, J., Izarra, C., 2002. The crustal structure of the Guayana Shield, Venezuela, from seismic refraction and gravity data. *Tectonophysics* **345**, 103–118.

Schulze, D.J., 2003. A classification scheme for mantle-derived garnets in kimberlite: a tool for investigating the mantle and exploring for diamonds. *Lithos* **71**, 195–213.

Schulze, D.J., Valley, J.W., Spicuzza, M.J., Channer, D.M.DeR., 2003a. The oxygen isotope composition of eclogitic and peridotitic garnet xenocrysts from the La Ceniza kimberlite, Guaniamo, Venezuela. *Int. Geol. Rev.* **45**, 968–975.

Schulze, D.J., Harte, B., Valley, J.W., Brenan, J.M., Channer, D.M.DeR., 2003b. Extreme crustal oxygen isotope signatures preserved in coesite in diamond. *Nature* **423**, 68–70.

Sidder, G.B., Mendoza, V., 1995. Geology of the Venezuelan Guayana Shield and its relation to the geology of the entire Guayana Shield. *U.S. Geol. Surv. Bull.* **2124**, B1–B41.

Sobolev, N.V., Efimova, E.S., Channer, D.M.DeR., Anderson, P.F.N., Barron, K.M., 1998. Unusual upper mantle beneath Guaniamo, Guyana Shield, Venezuela: evidence from diamond inclusions. *Geology* **26**, 971–974.

Sun, S.-S., McDonough, W.F., 1989. Chemical and isotopic systematics of oceanic basalts: implications for mantle composition and processes. In: Saunders, A.D., Norry, A.J. (Eds.), *Magmatism in the Ocean Basins*. Geol. Soc. Spec. Pub., London, pp. 313–345.

Vearncombe, S., Vearncombe, J.R., 2002. Tectonic controls on kimberlite location, southern Africa. *J. Struct. Geol.* **24**, 1619–1625.